

Collision-inclusive Manipulation Planning for Occluded Object Grasping via Compliant Robot Motions

Kejia Ren¹, Gaotian Wang¹, Andrew S. Morgan², and Kaiyu Hang¹

Abstract—Traditional robotic manipulation mostly focuses on collision-free tasks. In practice, however, many manipulation tasks (e.g., occluded object grasping) require the robot to intentionally collide with the environment to reach a desired task configuration. By enabling compliant robot motions, collisions between the robot and the environment are allowed and can thus be exploited, but more physical uncertainties are introduced. To address collision-rich problems such as occluded object grasping while handling the involved uncertainties, we propose a collision-inclusive planning framework that can transition the robot to a desired task configuration via roughly modeled collisions absorbed by Cartesian impedance control. By strategically exploiting the environmental constraints and exploring inside a manipulation funnel formed by task repetitions, our framework can effectively reduce physical and perception uncertainties. With real-world evaluations on both single-arm and dual-arm setups, we show that our framework is able to efficiently address various realistic occluded grasping problems where a feasible grasp does not initially exist.

I. INTRODUCTION

Traditional robotic manipulation research in motion and grasp planning relies strongly on the assumption that a collision-free solution exists. In those paradigms, the robot must compute and then effectively follow a path through free space, avoiding all collisions, in order to reach the desired task configuration [1]–[3]. However, in many practical scenarios (e.g., grasping a wide object on a flat surface, and tightly stacked books) showcased in Fig. 1, a collision-free grasp configuration does not initially exist due to occlusions by surrounding objects, and traditional collision-free strategies cannot find a solution. In contrast, like how humans grasp in such configurations, by allowing collisions and safe interactions between the gripper and the environment, the robot can insert its fingers into narrow gaps between objects to create free space for a desired grasp. For example, in Fig. 1, the robot can insert one finger in between the object and the table surface to scoop-grasp a wide object; or insert both fingers into gaps between books to grasp the target one.

Such collision-inclusive strategies require safe contact and effective interactions between the robot and the objects, for which robot compliance is essential [4]. More recently, by novel hand designs with soft material and actuators [5], [6] or impedance-controlled motion strategies [7], robot compliance has been more extensively investigated and exploited for contact-rich manipulation. Although compliance enables robots to have more manipulation possibilities, it

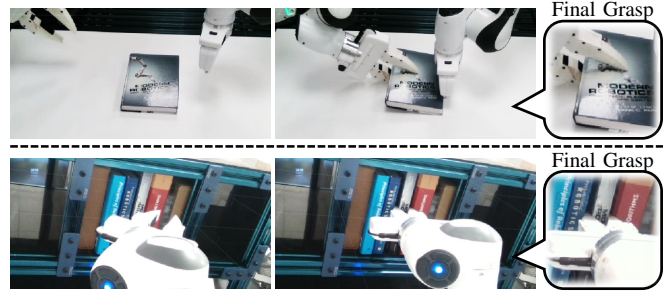


Fig. 1: Illustrations of occluded grasping tasks solved by our proposed collision-inclusive planner. *Top*: A book is lying flat on a table surface, needing the robot gripper to scoop-grasp it by contacting the table. *Bottom*: A target book is tightly surrounded by other books on the shelf, requiring the robot gripper to insert its fingers into the gaps between books for a stable grasp.

also introduces more uncertainties to make the task execution more challenging. In fact, exploiting environmental constraints (e.g., using contacts via compliance) can compensate for uncertainties to generate more robust manipulation outcomes [8]. For the example scenarios shown in Fig. 1, with inaccurate object pose estimation and uncertain robot execution of compliant motions, directly placing the fingertip at the narrow gap and precisely navigating it through the gap to reach a desired grasp pose is almost impossible. Instead, by maintaining continuous contact with the environment (e.g., the table surface or the surrounding books), the motion of the robot gripper will be constrained by the environment, and the transition of system state will become more certain; As a result, the finger will successfully slide into the target gap while moving along the environmental surfaces.

In addition, the idea of *Manipulation Funnels* has been studied to robustly manipulate objects against uncertainties, e.g., the variations in initial task configurations [9]. In this work, inspired by a broadened interpretation of manipulation funnels, we leverage repeated actions to produce stable manipulation outcomes under uncertainties. With minor variations across different trials, task repetitions conceptually explore in a manipulation funnel to effectively guide the manipulation through desired motion transitions and find the solution. More details will be discussed in Sec. III.

Motivated by the insights above, in this work, we propose a framework for occluded object grasping for which the feasible grasp configuration is initially blocked by the environment. Given mesh models of the robot gripper and the objects, our collision-inclusive framework is able to:

- 1) robustly move the robot to the desired task configuration without accurate system modeling and perception;

¹KR, GW, and KH are with the Department of Computer Science, Rice University, Houston, TX 77005, USA. KH is also with the Ken Kennedy Institute at Rice University. This project is supported by NSF-2240040.

²ASM is with The AI Institute, Cambridge, MA 02142, USA.

- 2) generate effective compliant motions that exploit environmental constraints to reduce task uncertainties;
- 3) produce more stable task outcomes through exploring a manipulation funnel formed by repeated actions.

II. RELATED WORK

Occluded Object Grasping. When all feasible grasp configurations for the target object are occluded by the environment or surrounding objects, traditional collision-free motion and grasp planning frameworks cannot solve the problem. In such scenarios, the robot needs to reconfigure the objects to certain desired configurations where a grasp can be achieved. To this end, object rearrangement via nonprehensile actions such as pushing can be incorporated for pre-grasp manipulation [10], [11]. By manually designed primitives or learned policies, other motion skills such as sliding the object to the table edge [12], [13] or the wall [14] and flipping the object against the wall [15]–[17] can also be leveraged. Unlike the existing strategies which require significant reconfiguration of the objects, this work addresses the occluded grasping problem in a confined space without much object motions, via collision-inclusive compliant actions.

Manipulation Funnels. The idea of manipulation funnels was originally proposed in [9] to robustly manipulate objects despite variations in their initial locations and shapes. The idea was later followed by other early works for peg-in-hole [18], door-closing [19], and parts-feeding [20] applications. However, their funnels were limited to only geometric funnels. More recent work has explored manipulation funnels by empirical analysis [21], and robust in-hand manipulation can be accomplished via the compositions of funnels [22]. In our framework, we broaden the idea of funnels and explore the manipulation funnel formed by repeated actions: With variations in the initial manipulation states (e.g., different gripper poses relative to the object), task repetitions will implicitly eliminate the involved uncertainties and produce stable outcomes (e.g., a desired grasp) after a few trials.

Exploitation of Environmental Constraints. Exploiting environmental constraints (e.g., through motions in contact with the environment), also known as extrinsic dexterity [23], has been extensively investigated to reduce execution uncertainties during manipulation [24]. Such a concept has been successfully applied in various manipulation problems to generate robust solutions in grasping [8], [25] and in-hand manipulation [23]. Furthermore, environmental constraints can also facilitate the learning of manipulation skills [26]–[28] for improved robustness and generalizability. In this work, we exploit environmental constraints to reduce the uncertainties caused by inaccurate sensing and approximate dynamics modeling, for robust compliant manipulation.

III. PROBLEM STATEMENT

In this work, we are interested in planning compliant motions of a robot manipulator in a collision-rich environment, to grasp a target object whose stable grasping configuration is originally occluded by other objects in the environment. For such reasons, the robot has to 1) physically interact

with the environment by making safe collisions with it; 2) create free space without greatly changing the environment configuration; and 3) insert its gripper into the desired grasp pose which is originally infeasible due to occlusions.

A. Preliminaries

The configuration of a robot at time t is represented by its joint angles $\mathbf{q}_t \in \mathbb{R}^N$ where N is the degrees-of-freedom (DoF) of the robot. We specify a workspace with respect to the robot’s base frame. A task frame is defined on the robot gripper and we denote the $SE(3)$ pose of this frame in the workspace (i.e., the robot’s base frame) by $\mathbf{x}_t \in \mathbb{R}^6$ (i.e., position and orientation represented by roll, pitch, and yaw angles), which can be obtained by forward kinematics of the robot $\mathbf{x}_t = \text{FK}(\mathbf{q}_t)$. Furthermore, We use the capital notation $\mathbf{X}_t \in SE(3)$ to represent the pose of the task frame (i.e., \mathbf{x}_t) as a transformation matrix. Given a point $\mathbf{p} \in \mathbb{R}^3$ in the task frame, the operation $\mathbf{X}_t \cdot \mathbf{p}$ calculates transformed coordinates of this point in the robot’s base frame. In this work, since the occluded grasping tasks require the robot to insert its fingers into narrow gaps between objects, the task frame is defined at one of the fingertips of the gripper.

An impedance control (commanded to the robot) is modeled by a reference equilibrium pose $\boldsymbol{\xi} \in SE(3)$ for the task frame, and its associated stiffness and damping parameters $\mathbf{K}, \mathbf{D} \in \mathbb{R}^{6 \times 6}$. By setting the equilibrium pose to $\boldsymbol{\xi}$ in the workspace, a Cartesian impedance controller virtually exerts a wrench $\mathbf{f}_t \in \mathbb{R}^6$ (including 3D force and torque) at the task frame (i.e., gripper’s fingertip) to perform a robot Cartesian behavior mimicking a virtual spring-damping system:

$$\mathbf{f}_t = \mathbf{K} (\boldsymbol{\xi} - \mathbf{x}_t) - \mathbf{D} \dot{\mathbf{x}}_t \quad (1)$$

where $\dot{\mathbf{x}}_t \in \mathbb{R}^6$ is the velocity of the task frame. The robot state will then evolve under the impedance-controlled dynamics as follows:

$$\mathbf{M}(\mathbf{q}_t) \ddot{\mathbf{q}}_t + \mathbf{C}(\mathbf{q}_t, \dot{\mathbf{q}}_t) = \mathbf{J}(\mathbf{q}_t)^\top (\mathbf{f}_t + \mathbf{f}_{ext}) \quad (2)$$

where $\dot{\mathbf{q}}_t, \ddot{\mathbf{q}}_t \in \mathbb{R}^N$ are the joint velocities and accelerations of the robot; $\mathbf{M}(\mathbf{q}_t) \in \mathbb{R}^{N \times N}$ is the mass matrix; $\mathbf{C}(\mathbf{q}_t, \dot{\mathbf{q}}_t) \in \mathbb{R}^N$ contains the centrifugal and Coriolis terms; $\mathbf{J}(\mathbf{q}_t) \in \mathbb{R}^{6 \times N}$ is the Jacobian matrix; $\mathbf{f}_{ext} \in \mathbb{R}^6$ is an external wrench received by the robot at the task frame.

The task environment contains M objects of interest $\{\mathcal{O}_1, \dots, \mathcal{O}_M\}$, where $\mathcal{O}_i \subset \mathbb{R}^3$ represents the geometry of the i -th object. The pose of the i -th object in the workspace (i.e., the robot’s base frame) is denoted by $\mathbf{X}^i \in SE(3)$ as a transformation matrix. One of the objects, $g \in \{1, \dots, M\}$ is the target object to be grasped; the geometry and pose of the target object are denoted by $\mathcal{O}^g \subset \mathbb{R}^3$ and $\mathbf{X}^g \in SE(3)$ respectively. Given the geometry of the target object, a stable grasp pose $\mathbf{X}^* \in SE(3)$ for the task frame (of the robot gripper) can be obtained by an off-the-shelf grasp planning algorithm, which is expressed in the target object’s body frame. To express this grasp pose in the robot’s base frame, we need to transform it by $\mathbf{X}^g \cdot \mathbf{X}^*$, where the operator \cdot is matrix multiplication for transformation matrices.

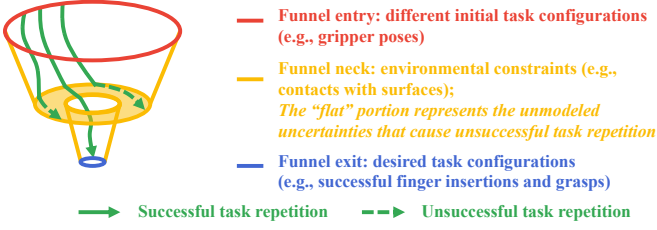


Fig. 2: Degenerate manipulation funnel by repetitions.

We aim to find a sequence of Cartesian impedance controls, represented by a sequence of reference equilibrium poses $\{\xi_0, \dots, \xi_{T-1}\}$ of task frame, to move the robot gripper to reach the desired (yet initially occluded) grasp pose $\mathbf{X}^g \cdot \mathbf{X}^*$ from a starting collision-free pose $\mathbf{X}_0 \in SE(3)$ through safe contacts and interactions with the environment.

B. Exploring in Manipulation Funnel by Repetitions

The impedance controls are generated in an open loop and may not lead to a successful task completion during real executions, due to physical and perception uncertainties. However, as the failed execution does not greatly change the environment configuration, a repeated execution with some local randomness is still likely to achieve the task. To this end, our framework allows the robot to attempt more trials with repeated actions. Conceptually, as shown in Fig. 2, we can formulate a degenerate manipulation funnel that allows repeated actions to enter and navigate through. The entry of the funnel is defined by all initial task configurations (e.g., gripper poses, minor variations in object shape and poses); the exit of the funnel is all desired task completion states (e.g., stable grasps); the neck is the environmental or other task-implicit constraints that transition the manipulation towards the desired states. Each task repetition planned using environmental constraints is a series of motions that go inside the funnel from its entry towards the exit. Due to inaccurate modeling and uncertainties (as represented by the “flat” degenerate funnel neck in the figure), a repetition may not successfully find the funnel exit. However, the repetitions are always contained inside the funnel by not greatly disrupting the environment configuration and constraints. With more valid repetitions, the manipulation will finally locate the funnel exit to robustly finish the task.

Our proposed framework is outlined in Alg. 1. Specifically, the framework first observes the poses of objects in the environment. Provided with a desired grasp pose \mathbf{X}^* , a starting collision-free pre-grasp pose \mathbf{X}_0 of the gripper will be sampled around the workspace. To move the task frame of the robot gripper from \mathbf{X}_0 to the desired grasp $\mathbf{X}^g \cdot \mathbf{X}^*$, our collision-inclusive planner will then generate a sequence of desired impedance controls in two steps: 1) by exploiting environmental constraints (e.g., contacts with the objects or support surfaces), a geometric path will be planned for the task frame in Sec. IV-B; 2) Guided by the geometric path planned in the previous step, a sequence of impedance controls, represented by equilibrium poses for the task frame, will be generated via optimization in Sec. IV-C.

Algorithm 1 Collision-inclusive Manipulation Planning

Input: Object geometries $\{\mathcal{O}_1, \dots, \mathcal{O}_M\}$ where $g \in \{1, \dots, M\}$ is the index of the target object, desired grasp pose of the robot gripper’s task frame \mathbf{X}^* specified in the target object’s body frame, maximum number of repetitions K_{\max}

Output: Task success (*true* or *false*)

```

1:  $k \leftarrow 0$  ▷ Number of Repetitions
2: while  $k < K_{\max}$  do
3:    $k \leftarrow k + 1$ 
4:    $\{\mathbf{X}^1, \dots, \mathbf{X}^M\} \leftarrow \text{OBSERVE}()$  ▷ Object Poses
5:    $\mathbf{X}_0 \leftarrow \text{SAMPLEAROUND}(\mathbf{X}^g \cdot \mathbf{X}^*)$ 
6:    $\{\tilde{\mathbf{X}}_t\}_{t=1}^T \leftarrow \text{GEOMPATH}(\mathbf{X}_0)$  ▷ Sec. IV-B
7:    $\{\xi_t\}_{t=0}^{T-1} \leftarrow \text{IMPDCtrl}(\{\tilde{\mathbf{X}}_t\}_{t=1}^T)$  ▷ Sec. IV-C
8:    $\text{MOVEGRIPPERTO}(\mathbf{X}_0)$ 
9:   if  $\text{EXECUTE}(\{\xi_0, \dots, \xi_{T-1}\})$  then
10:    return true
11:   end if
12: end while
13: return false

```

The generated impedance controls will be commanded to the robot for execution. Meanwhile, if the task frame greatly deviates from the planned geometric path in Step 1), we will early terminate the execution by returning a *false* in the $\text{EXECUTE}(\cdot)$ function and skip to the next trial. After all impedance controls have been executed, the robot will close its gripper to grasp the target object. If the grasp is stable, as assessed by some off-the-shelf grasping criteria, the task is completed; otherwise, the robot will open the gripper, move to a newly sampled pre-grasp pose \mathbf{X}_0 , and start the next trial. The repetition continues until the target object is stably grasped or the number of trials exceeds a preset limit K_{\max} .

IV. COLLISION-INCLUSIVE PLANNING

Given the geometric modeling of the robot gripper and environmental objects as will be described in Sec. IV-A, this section introduces the procedure and details how the framework generates impedance controls through optimization-based planning, as will be detailed in Sec. IV-B and IV-C.

A. Geometric Representations of Robot and Objects

When planning and executing interactive robot motions, an efficient computation of the distance between the robot and environmental objects is needed. The exact computation of distance between complex mesh models in 3D space can be expensive and non-differentiable. Therefore, appropriate approximate geometric representations of the robot and objects are needed to facilitate efficient distance computation between shapes. As shown in Fig. 3 (left), we approximately represent the geometry of the robot gripper by a point cloud sampled on the gripper’s mesh model, i.e., $\mathcal{P} \subset \mathbb{R}^3$, where the coordinates of each point $\mathbf{p} \in \mathcal{P}$ is given in the task frame of the gripper. The points are sampled both on the surface and inside the volume of the gripper’s mesh model, i.e., $\mathcal{P} = \mathcal{P}^s \cup \mathcal{P}^v$ where \mathcal{P}^s and \mathcal{P}^v contain points sampled on the surface of and inside the mesh respectively.

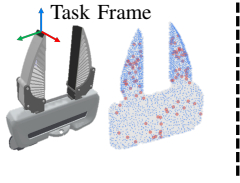


Fig. 3: *Left*: The gripper’s geometry is represented by a point cloud, randomly sampled on both the surface (blue) and inside the volume (red) of the mesh model. The task frame is defined at one fingertip. *Right*: The object (i.e., mustard bottle) is geometrically modeled by a signed distance field (SDF), where positive and negative values are visualized by yellow and green points respectively.

For each object \mathcal{O}_i , we generate a discrete signed distance field (SDF). We first sample a 3D grid with a resolution of Δ around the object; then, we compute the signed distance value for each voxel of the grid to construct a discrete SDF, as shown in Fig. 3 (right). Given an arbitrary query point $\mathbf{p} \in \mathbb{R}^3$ in the object’s body frame, the signed distance of this query point can be approximated by interpolating values on the discrete SDF grid, which we denote by $\text{SDF}_i(\mathbf{p}) \in \mathbb{R}$. To infer the signed distance of a point \mathbf{p} given in the robot’s base frame, we define a function $\phi_i : \mathbb{R}^3 \mapsto \mathbb{R}$, which queries the SDF after transforming this point into the object’s body frame using the observed object’s pose $\mathbf{X}^i \in SE(3)$:

$$\phi_i(\mathbf{p}) = \text{SDF}_i\left(\left(\mathbf{X}^i\right)^{-1} \cdot \mathbf{p}\right) \quad (3)$$

In addition, to obtain the signed distance of a point \mathbf{p} (given in the robot’s base frame) to the whole environment consisting of all objects, we define another function $\phi : \mathbb{R}^3 \mapsto \mathbb{R}$ by taking the signed distance to its nearest object:

$$\phi(\mathbf{p}) = \min_{i \in \{1, \dots, M\}} \phi_i(\mathbf{p}) \quad (4)$$

B. Constraint-Exploiting Geometric Path Planning

Precisely placing the robot finger to a narrow gap for pre-grasp insertion merely based on visual perception is not reliable due to perceptual uncertainty. Instead, locally exploring and exploiting the environmental constraints (e.g., touching and sliding on the environmental surfaces) is more robust to such uncertainties for locating the gaps. For example, when inserting a finger into the gap between two tightly stacked books as shown in Fig. 4, directly hitting the finger toward the gap from in the air based on purely visual perception is likely to miss it since the gap’s location can be inaccurately observed. However, if we let the robot slide its finger on the book surface near the gap, the robot can more robustly find the gap by trapping its finger in the gap during sliding. Based on this intuition, we expect the task frame (at the fingertip) to follow a geometric path that actively exploits environmental constraints by contacting the object surfaces, as shown in Fig. 4. Meanwhile, we also want to reduce collisions between the environment and other parts (e.g., the gripper base) of the robot gripper, since unexpected contacts can easily deviate the gripper from its desired motion behavior while the robot moves compliantly. Taking into account both aspects, we propose to generate a desired geometric path for the gripper’s task frame in two steps:

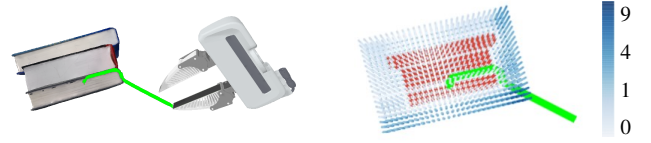


Fig. 4: Positional path-finding via A^* algorithm illustrated with a book-grasping example. *Left*: The fingertip of the gripper (i.e., the task frame) needs to follow a desired positional path (green), to exploit environmental constraints (i.e., contacts with object surfaces) for a more robust insertion into the gap between books. *Right*: The desired positional path (green) is planned on the 3D discretized workspace using an A^* algorithm. The red grids penetrate the environment by a preset threshold δ_g and are regarded as obstacles. The colors of the blue grids (i.e., non-obstacle grids) represent their squared signed distance values, i.e., $\phi(\mathbf{p})^2$, in cm^2 .

1) *Positional Path-Finding via A^* Algorithm*: As the first step, we plan only the positional motions of the fingertip, which will be used as a guidance to plan the entire pose path (i.e., position and orientation) in the next step. To exploit environmental constraints, we want the task frame (fingertip) to get close enough to the environmental surface and contact it, but not to penetrate too much into the environment to be performed in reality. Particularly, the positional path-finding for the task frame is formulated as an optimization problem:

$$\underset{\mathbf{p}_1, \dots, \mathbf{p}_T}{\text{minimize}} \quad w \cdot \sum_{t=1}^T \phi(\mathbf{p}_t)^2 + \sum_{t=0}^{T-1} \|\mathbf{p}_t - \mathbf{p}_{t+1}\|^2 \quad (5a)$$

$$\text{subject to} \quad \phi(\mathbf{p}_t) + \delta_g \leq 0, \quad \forall t = 1, \dots, T \quad (5b)$$

where the first term in the objective of Eq. (5a) is squared SDF to encourage the fingertip to touch environmental surfaces, and the second term is a smoothing term; w is a scaling factor to trade-off between two terms in the objective, which we set to $w = 1/\Delta^2$ for all our experiments (Δ is the grid resolution of SDF). By setting a nonnegative threshold δ_g in the constraint Eq. (5b), we ensure the fingertip will not penetrate the environment too much.

We solve the above path-finding problem by searching via an A^* algorithm over the 3D workspace, as illustrated in Fig. 4 (right). Specifically, we discretize the workspace containing objects into a 3D grid with a resolution of Δ . For the grids whose coordinates penetrate the environment by a value greater than δ_g , i.e., violating the constraint in Eq. (5b), we regard this grid as being an obstacle to prevent the path from passing through it. For two neighbor grids with coordinates \mathbf{p} and \mathbf{p}' , the cost is defined as $c(\mathbf{p}, \mathbf{p}') = w \cdot \phi(\mathbf{p}')^2 + \|\mathbf{p} - \mathbf{p}'\|^2$; and the heuristic function is simply the smoothing term (i.e., the path length), i.e., $h(\mathbf{p}, \mathbf{p}') = \|\mathbf{p} - \mathbf{p}'\|^2$, which underestimates the cost to ensure optimality of the found path. If the A^* algorithm finds a path, represented by a sequence of traversed grids, we will interpolate it with T waypoints to extract a positional path $\{\mathbf{p}_1, \dots, \mathbf{p}_T\}$ as the solution to Eq. (5).

It is worth noting that the threshold δ_g for allowed penetration is important for the existence of a solution. As detailed in Alg. 2, we run our A^* with an initial δ_g . If the path does not exist, we will relax the allowed penetration δ_g by iteratively increasing it by $d\delta_g$, until a path is found.

Algorithm 2 Iterative Path-Finding via A^* Algorithm

Input: Initial δ_g , increment step $d\delta_g$
Output: The found path $\{\mathbf{p}_1, \dots, \mathbf{p}_T\}$
1: **while** *true* **do**
2: $path \leftarrow \text{ASTARALG}(\delta_g)$ \triangleright Over a 3D Grid Workspace
3: **if** $path$ is not *null* **then**
4: $\{\mathbf{p}_1, \dots, \mathbf{p}_T\} \leftarrow \text{INTERPOLATE}(path)$
5: **return** $\{\mathbf{p}_1, \dots, \mathbf{p}_T\}$
6: **end if**
7: $\delta_g \leftarrow \delta_g + d\delta_g$
8: **end while**

2) *Optimization-based Path Refinement via Collision Minimization:* In the second step, we aim to minimize collisions between the gripper and the environment, while still keeping the fingertip following the constraint-exploiting path found in the previous step. For this, we define a collision cost similar to CHOMP [29]. Given the signed distance $\phi(\mathbf{p}) \in \mathbb{R}$ of a point $\mathbf{p} \in \mathbb{R}^3$, the collision cost is defined as follows:

$$c(\phi(\mathbf{p})) = \begin{cases} -\phi(\mathbf{p}) + \frac{1}{2}\varepsilon & \phi(\mathbf{p}) < 0 \\ \frac{1}{2\varepsilon}(\phi(\mathbf{p}) - \varepsilon)^2 & 0 \leq \phi(\mathbf{p}) < \varepsilon \\ 0 & \text{otherwise} \end{cases} \quad (6)$$

Given the pose $\mathbf{X}_t \in SE(3)$ of the task frame, the overall collision cost is computed by summing for each object i and each sampled point $\mathbf{p} \in \mathcal{P}^v$ within the gripper's volume:

$$C(\mathbf{X}_t) = \sum_{i=1}^M \sum_{\mathbf{p} \in \mathcal{P}^v} c(\phi_i(\mathbf{X}_t \cdot \mathbf{p})) \quad (7)$$

where $\mathbf{X}_t \cdot \mathbf{p}$ transform a point $\mathbf{p} \in \mathcal{P}^v$ defined in the task frame to the robot's base frame.

Then, guided by the positional path $\{\mathbf{p}_1, \dots, \mathbf{p}_T\}$ found in the previous step, we refine to obtain the geometric path $\{\tilde{\mathbf{X}}_1, \dots, \tilde{\mathbf{X}}_T\}$ where $\tilde{\mathbf{X}}_t \in SE(3)$ (i.e., containing both positions and orientations), by minimizing the collision cost in a constrained optimization problem in Eq. (8):

$$\underset{\tilde{\mathbf{X}}_1, \dots, \tilde{\mathbf{X}}_T}{\text{minimize}} \quad \sum_{t=1}^T C(\tilde{\mathbf{X}}_t) + \sum_{t=0}^{T-1} d(\tilde{\mathbf{X}}_t, \tilde{\mathbf{X}}_{t+1}) \quad (8a)$$

$$\text{subject to} \quad \tilde{\mathbf{X}}_T = \mathbf{X}^g \cdot \mathbf{X}^* \quad (8b)$$

$$\|\tilde{\mathbf{p}}_t - \mathbf{p}_t\| \leq \delta_p, \quad \forall t \in \{1, \dots, T\} \quad (8c)$$

where the first term of the objective Eq. (8a) is the collision cost; the second is a distance smoothing term; the constraint in Eq. (8b) is to ensure the final pose of the solution reaches the desired grasp pose; the constraint in Eq. (8c) prevents the solution geometric path from deviating from the constraint-exploiting positional path $\{\mathbf{p}_t\}_{t=1}^T$ found in the first step (note: $\tilde{\mathbf{p}}_t \in \mathbb{R}^3$ denotes the positional component of $\tilde{\mathbf{X}}_t$).

C. Impedance Control Generation

After a desired geometric path has been planned in Sec. IV-B, we need to find a sequence of impedance controls $\{\xi_0, \dots, \xi_{T-1}\}$ to drive the robot's gripper to follow the desired geometric path, by using robot dynamics as a heuristic. In Eq. (2), the value of term $C(\mathbf{q}_t, \dot{\mathbf{q}}_t)$ can be observed

in real time; this term can be canceled from the dynamics equation by implementing an internal Coriolis-compensating mechanism for the controller. Then, by substituting $\ddot{\mathbf{x}} = \mathbf{J}\dot{\mathbf{q}} + \dot{\mathbf{J}}\dot{\mathbf{q}}$ into Eq. (2) of robot dynamics, the impedance-controlled behavior of the task frame can be inferred:

$$\Lambda(\mathbf{q}_t) \left(\ddot{\mathbf{x}}_t - \dot{\mathbf{J}}(\mathbf{q}_t) \dot{\mathbf{q}}_t \right) = \mathbf{f}_t + \mathbf{f}_{ext} \quad (9)$$

where $\Lambda(\mathbf{q}_t) = \mathbf{J}(\mathbf{q}_t)^{-\top} \mathbf{M}(\mathbf{q}_t) \mathbf{J}(\mathbf{q}_t)^{-1}$ is the effective inertia matrix of robot in the task space. When the robot moves locally with a slow speed, we can ignore the effect of term $\dot{\mathbf{J}}(\mathbf{q}_t) \dot{\mathbf{q}}_t$. Then, we can obtain a highly approximated yet computationally less expensive dynamics equation, to heuristically guide the generation of impedance controls:

$$\ddot{\mathbf{x}}_t \approx \Lambda(\mathbf{q}_t)^{-1} (\mathbf{f}_t + \mathbf{f}_{ext}) \quad (10)$$

The external wrench $\mathbf{f}_{ext} \in \mathbb{R}^6$ is estimated based on the virtual penetration along the planned geometric path. Specifically, when the gripper is at pose $\tilde{\mathbf{X}}_t$ while following the geometric path, a local force $\mathbf{f}(\mathbf{p}) \in \mathbb{R}^3$ can be estimated at each point $\mathbf{p} \in \mathcal{P}^s$ sampled on the gripper's surface. The force $\mathbf{f}(\mathbf{p})$ has a magnitude proportional to the penetration distance (i.e., the negative of signed distance) from this point to the environment; the direction of $\mathbf{f}(\mathbf{p})$ is the same as the normal direction of the gripper surface at this point:

$$\mathbf{f}(\mathbf{p}) = \mathbb{1}_{\{\phi(\tilde{\mathbf{X}}_t \cdot \mathbf{p}) < 0\}} \cdot k\phi(\tilde{\mathbf{X}}_t \cdot \mathbf{p}) \cdot \mathbf{n} \quad (11)$$

where $\phi(\tilde{\mathbf{X}}_t \cdot \mathbf{p})$ is the signed distance from a point \mathbf{p} (on the gripper's surface) to the environment; the indicator function $\mathbb{1}_{\{\phi(\tilde{\mathbf{X}}_t \cdot \mathbf{p}) < 0\}}$ filters out the points not in penetration since such points will not exert forces; k is a hyperparameter corresponding to the stiffness of virtual penetrations; $\mathbf{n} \in \mathbb{R}^3$ is the outward normal vector of the gripper's geometric model at point \mathbf{p} . Then, the estimated external wrench \mathbf{f}_{ext} (i.e., force and torque) received by the gripper is obtained by averaging the effect of local force at each point:

$$\mathbf{f}_{ext}(\tilde{\mathbf{X}}_t) = \frac{1}{Z} \left(\begin{array}{c} \tilde{\mathbf{R}}_t \cdot \sum_{\mathbf{p} \in \mathcal{P}^s} \mathbf{f}(\mathbf{p}) \\ \tilde{\mathbf{R}}_t \cdot \sum_{\mathbf{p} \in \mathcal{P}^s} \mathbf{p} \times \mathbf{f}(\mathbf{p}) \end{array} \right) \in \mathbb{R}^6 \quad (12)$$

where $Z = \sum_{\mathbf{p} \in \mathcal{P}^s} \mathbb{1}_{\{\phi(\tilde{\mathbf{X}}_t \cdot \mathbf{p}) < 0\}}$ calculates the number of points in penetration with the environment; $\tilde{\mathbf{R}}_t \in \mathbb{R}^{3 \times 3}$ is a rotation matrix corresponding to the orientational component of $\tilde{\mathbf{X}}_t$, which is used to transform the direction of force and torque to be expressed in the robot's base frame.

By integrating all the derived components above, we can give an estimated forward dynamics of the robot gripper under impedance control in a function $\Pi: \mathbb{R}^6 \times \mathbb{R}^6 \times \mathbb{R}^6 \mapsto \mathbb{R}^6 \times \mathbb{R}^6$, as expressed in Eq. (13). Given the gripper's pose \mathbf{x}_t and velocity $\dot{\mathbf{x}}_t$ and the impedance control ξ_t at time t (as defined in Sec. III-A), the function Π can infer the gripper's pose \mathbf{x}_{t+1} and velocity $\dot{\mathbf{x}}_{t+1}$ at the next time step:

$$\mathbf{x}_{t+1}, \dot{\mathbf{x}}_{t+1} = \Pi(\mathbf{x}_t, \dot{\mathbf{x}}_t, \xi_t) \quad (13)$$

which is calculated by taking integrals over the time $\tau \in [t, t+1]$ as follows:

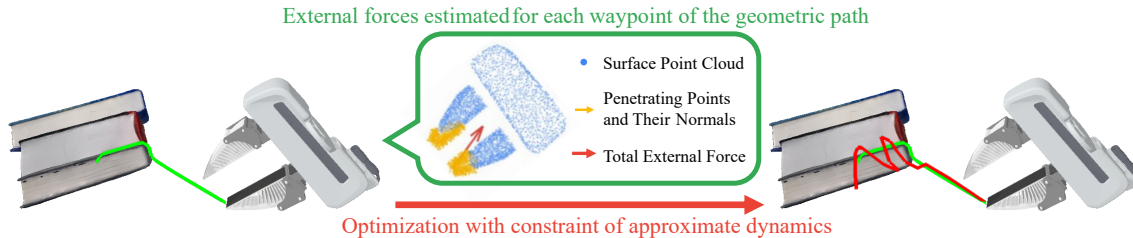


Fig. 5: Illustration of impedance control generation with a book-grasping example. The left figure shows the geometric path (green lines) found by the approach described in Sec. IV-B. In the middle figure, for each waypoint of the geometric path, an external force (red arrow) can be estimated by averaging the effects of penetrating points (yellow). The right figure shows the generated impedance controls (i.e., the red trajectory of equilibrium poses), solved by an optimization program constrained by the approximate dynamics.

$$\mathbf{x}_\tau = \mathbf{x}_t + \int_t^\tau \dot{\mathbf{x}}_\tau d\tau \quad (14a)$$

$$\dot{\mathbf{x}}_\tau = \dot{\mathbf{x}}_t + \int_t^\tau \ddot{\mathbf{x}}_\tau d\tau \quad (14b)$$

$$\ddot{\mathbf{x}}_\tau = \Lambda^{-1} \left(\mathbf{f}_\tau - \mathbf{f}_{ext}(\tilde{\mathbf{X}}_t) \right) \quad (14c)$$

$$\mathbf{f}_\tau = \mathbf{K}(\xi_t - \mathbf{x}_\tau) - \mathbf{D}\dot{\mathbf{x}}_\tau \quad (14d)$$

In practice, we evaluate the above integrals numerically at small time intervals of 2 milliseconds; the damping parameters are set to critical damping $\mathbf{D} = 2\sqrt{\mathbf{K}}$.

Finally, by incorporating the approximated dynamics Π as a heuristic constraint in Eq. (15d), the sequence of impedance controls can be generated by solving a constrained optimization program as expressed in Eq. (15). As visualized in Fig. 5, the program aims to have the controlled robot gripper follow the constraint-exploiting geometric path $\{\tilde{\mathbf{X}}_1, \dots, \tilde{\mathbf{X}}_T\}$ planned in Sec. IV-B. As such, the program's objective is to minimize the distance between the planned geometric path and the predicted path from impedance-controlled dynamics.

$$\text{minimize}_{\xi_0, \dots, \xi_{T-1}} \sum_{t=1}^T d(\tilde{\mathbf{X}}_t, \mathbf{X}_t) \quad (15a)$$

$$\text{subject to } \|\dot{\mathbf{x}}_0\|^2 = 0, \quad \|\dot{\mathbf{x}}_T\|^2 = 0 \quad (15b)$$

$$\|\dot{\mathbf{x}}_t\|^2 \leq \delta_v, \quad \forall t = 1, \dots, T-1 \quad (15c)$$

$$\mathbf{x}_{t+1}, \dot{\mathbf{x}}_{t+1} = \Pi(\mathbf{x}_t, \dot{\mathbf{x}}_t, \xi_t), \forall t = 0, \dots, T-1 \quad (15d)$$

where the constraint in Eq. (15b) is a boundary condition to ensure the robot gripper starts and stops at zero velocity; Eq. (15c) limits the gripper's speed by a threshold δ_v to ensure the safety of its motions. The solution of the optimization program $\{\xi_0, \dots, \xi_{T-1}\}$, as a sequence of reference equilibrium poses in $SE(3)$ for the gripper's task frame, will be commanded one by one to a Cartesian impedance controller to compliantly move the robot for execution.

V. EXPERIMENTS

We conducted experiments on Franka Emika robots with both single-arm and dual-arm setups, to evaluate the effectiveness of our proposed framework against real-world challenges. We selected 9 objects for evaluation, as shown in Fig. 6. The selected objects greatly differ in their geometric and physical properties such as size, weight, stiffness, etc. We used a model-based 6D pose estimator FoundationPose [30]

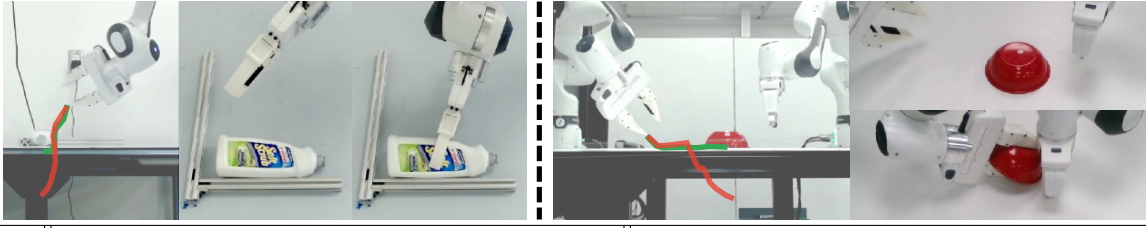
with CNOS [31] segmenting the objects on the first frame. The visual models were run on a single RTX 3060 GPU with 12 GB memory. Our collision-inclusive planner was implemented in Python with a single thread on a 3.4 GHz AMD Ryzen 9 5950X CPU; the involved optimization programs (i.e., in Sec. IV-B.2 and IV-C) were solved using the CasADi framework [32] with IPOPT solver (an interior point method). The length of the planned path or trajectory (i.e., the number of execution steps) was always set to $T = 20$.



Fig. 6: The objects selected for evaluation: 1. Book [33]; 2. Cleanser Bottle (YCB #20); 3. Mustard Bottle (YCB #9); 4. Cracker Box (YCB #1); 5. Timer (YCB #71); 6. Clamp (YCB #46); 7. Scissors (YCB #35); 8. Bowl (YCB #25); 9. Plate (YCB #24). [34]

A. Grasping Single Object on a Support Surface

With both single-arm and dual-arm setups, we evaluated our proposed framework in grasping a single object on a flat table, as exemplified in Fig. 7. This task requires the robot to successfully insert one of its fingers into the narrow gap between the object and the table plane, where collisions are inevitable. To robustly find the gap and place the finger there, our framework automatically exploited environmental constraints by contacting the environmental objects, as showcased in Fig. 7. Our framework assumes that the environment configuration cannot be greatly changed by the robot, to keep the task configuration consistent as modeled by our framework. Therefore, for the single-arm setup, we constructed an aluminum frame and statically attached it to the table to constrain the motion range of objects; for the dual-arm setup, we commanded one robot arm to block the object from the opposite side of the grasping direction. The dual-arm experiments show promising feasibility of applying our framework in more realistic setups where the desired



Object	Single-Arm						Dual-Arm					
	Success	Reps (\pm std)	Solve Time (seconds)				Success	Reps (\pm std)	Solve Time (seconds)			
			A*	Refine	Impd	Total (\pm std)			A*	Refine	Impd	Total (\pm std)
Book	10 / 10	1.4 \pm 0.8	0.23	1.21	2.44	3.87 \pm 0.68	10 / 10	1.1 \pm 0.3	0.20	1.15	2.27	3.62 \pm 2.35
Cleanser	10 / 10	1.1 \pm 0.3	0.24	0.37	2.35	2.96 \pm 0.74	10 / 10	1.2 \pm 0.6	0.98	0.35	1.96	3.29 \pm 2.72
Mustard	10 / 10	1.0 \pm 0.0	0.16	0.46	2.54	3.16 \pm 0.86	10 / 10	1.3 \pm 0.9	6.87	0.31	1.93	9.11 \pm 3.90
Cracker	10 / 10	2.7 \pm 1.6	1.87	1.35	2.16	5.39 \pm 4.14	10 / 10	2.3 \pm 2.0	3.37	0.16	2.11	5.64 \pm 3.55
Timer	10 / 10	1.1 \pm 0.3	0.16	0.33	1.88	2.37 \pm 0.76	10 / 10	1.4 \pm 0.9	6.29	0.83	1.82	8.95 \pm 4.52
Clamp	10 / 10	1.1 \pm 0.3	0.16	0.36	2.23	2.75 \pm 0.61	10 / 10	1.2 \pm 0.4	0.20	0.39	2.17	2.76 \pm 0.60
Scissors	10 / 10	1.4 \pm 0.7	0.13	2.23	1.99	4.35 \pm 3.37	10 / 10	1.5 \pm 0.8	0.35	1.21	1.80	3.36 \pm 2.82
Bowl	10 / 10	1.6 \pm 0.7	0.05	0.49	1.91	2.45 \pm 0.71	10 / 10	3.3 \pm 1.6	0.20	0.60	1.96	2.76 \pm 1.46
Plate	10 / 10	1.0 \pm 0.0	0.05	0.32	2.19	2.57 \pm 0.69	10 / 10	1.1 \pm 0.3	0.05	0.48	2.34	2.86 \pm 1.26
Average	10 / 10	1.4 \pm 0.9	0.52	0.90	2.17	3.60 \pm 2.63	10 / 10	1.6 \pm 1.2	1.97	0.59	2.02	4.58 \pm 3.66

Fig. 7: Grasping a single object on a flat table surface by our framework, with both single-arm (left) and dual-arm (right) setups. The green lines show the geometric paths planned by the algorithms in Sec. IV-B, to exploit environmental constraints. Guided by the geometric paths and compensating against estimated external forces, desired impedance controls (red trajectories) are generated to compliantly move the gripper. The table shows evaluation results on 9 selected objects, where “Reps” is the average number of repetitions before success; the solve times of “A*”, “Refine”, and “Impd” correspond to the algorithmic steps described in Sec. IV-B.1, IV-B.2, and IV-C respectively.

constraints are not always naturally available and need to be constructed by the robot itself. We ran 10 trials for each selected object; for each trial, the maximum number of repetitions was set to $K_{\max} = 10$. The trial was logged as a failure if the object was not grasped within 10 repetitions.

We reported the experiment results in the table of Fig. 7. In all experiment trials, our framework succeeded with a small number of needed repetitions (1.4 for the single-arm and 1.6 for the dual-arm setups on average), showing the high effectiveness of our framework in such task setups. Grasping the cracker box and the bowl generally required more repetitions than other objects. This is because their thicknesses are roughly equal to the width between robot fingers when wide open, and thus need the gripper to more precisely orient itself for insertion. Furthermore, the cracker box was empty and more easily deformed, which made the manipulation more difficult by introducing more unmodeled uncertainties. Although the task was not always accomplished for the first time, the task repetitions, as desirably contained in a conceptual manipulation funnel, always produced stable outcomes and would eventually reach the grasp. In terms of solve times, the replanning of each repetition required less than 5 seconds. The A*-based positional path-finding (corresponding to Sec. IV-B.1) usually ran fast (i.e., less than 0.5 seconds); however, due to perception errors, the object may be estimated to penetrate the table with a large negative clearance between them. Such perceptual inaccuracy could require our algorithm to run more iterations by increasing δ_g and to more exhaustively search over the entire workspace to find a feasible path, making the runtime of the iterative A* sometimes longer (e.g., more than 6 seconds).

B. Grasping from Tightly Stacked Multiple Objects

For this evaluation, we further challenged our framework with more complicated environment configurations, where

Scene	Success	Reps (\pm std)	Solve Time (seconds)			
			A*	Refine	Impd	Total (\pm std)
1	10 / 10	3.3 \pm 1.7	0.14	2.32	2.10	4.55 \pm 4.08
2	10 / 10	1.1 \pm 0.3	0.10	5.65	1.48	7.23 \pm 6.35
3	10 / 10	2.7 \pm 1.6	1.04	0.64	2.01	3.69 \pm 3.78

Fig. 8: Grasping a target book in three scenes of tightly packed configurations. The table shows evaluation results on each scene.

multiple objects were tightly packed in a limited space. Specifically, rather than inserting one finger beneath the object in Sec. V-A, this setup requires the robot to insert both fingers into separate gaps at the same time, requiring our framework to deal with more complicated collisions with the environment. We constructed three test scenes of grasping a target book with other books (or objects) snugly next to it to occlude the desired grasp configuration, as shown in Fig. 8: 1. From the tray with a single arm; 2. From the shelf with a single arm; 3. Stacked flat on the table with dual arms (the other arm blocking objects from the other side). For each scenario, we ran 10 trials with a maximum number of repetitions $K_{\max} = 10$. To enable the insertion of both fingers, before execution of each trial, the robot was asked to configure its finger so that the width between fingers was similar to the thickness of the target book.

The experiment results are reported in the table of Fig. 8. As can be seen from the results, our framework still effectively succeeded in all trials of all scenarios. Since the task

setup became more complicated in terms of the environment geometries and required interactions to be considered, the average number of repetitions slightly increased. The refinement step of geometric path planning took longer to run since the nonlinear optimizer needed more iterations to find the optimal solution for collision minimization when both fingers had to penetrate the environment. However, the total runtime of replanning for each repetition was about 4 to 7 seconds in different scenes, which is still practical in reality.

VI. CONCLUSION

In this work, we proposed a collision-inclusive manipulation planning framework for collision-rich tasks using compliant robot motions, where the desired task configuration (e.g., a stable grasp for the target object) is initially occluded. With real-world experiments on various test scenarios, we show that our framework can effectively address practical occluded grasping problems under uncertainties by exploiting environmental constraints and task repetitions. In the future, we plan to upgrade our framework by integrating real-time force-torque feedback and closing the loop more tightly with an MPC-based strategy, to generate more reactive actions.

REFERENCES

- [1] A. D. Dragan, N. D. Ratliff, and S. S. Srinivasa, "Manipulation planning with goal sets using constrained trajectory optimization," in *IEEE International Conference on Robotics and Automation (ICRA)*. IEEE, 2011, pp. 4582–4588.
- [2] L. Wang, Y. Xiang, and D. Fox, "Manipulation trajectory optimization with online grasp synthesis and selection," in *Robotics: Science and Systems*, 2020.
- [3] Y. Xiang, S. H. Allu, R. Peddi, T. Summers, and V. Gogate, "Grasping trajectory optimization with point clouds," in *IEEE International Conference on Intelligent Robots and Systems (IROS)*, 2024.
- [4] C. Eppner, R. Deimel, J. Alvarez-Ruiz, M. Maertens, and O. Brock, "Exploitation of environmental constraints in human and robotic grasping," *The International Journal of Robotics Research*, vol. 34, no. 7, pp. 1021–1038, 2015.
- [5] L. U. Odhner, L. P. Jentoft, M. R. Claffee, N. Corson, Y. Tenzer, R. R. Ma, M. Buehler, R. Kohout, R. D. Howe, and A. M. Dollar, "A compliant, underactuated hand for robust manipulation," *The International Journal of Robotics Research*, vol. 33, no. 5, pp. 736–752, 2014.
- [6] R. Deimel and O. Brock, "A novel type of compliant and underactuated robotic hand for dexterous grasping," *The International Journal of Robotics Research*, vol. 35, no. 1-3, pp. 161–185, 2016.
- [7] P. Balatti, D. Kanoulas, G. F. Rigano, L. Muratore, N. G. Tsarakakis, and A. Ajoudani, "A self-tuning impedance controller for autonomous robotic manipulation," in *IEEE International Conference on Intelligent Robots and Systems (IROS)*. IEEE, 2018, pp. 5885–5891.
- [8] C. Eppner and O. Brock, "Planning grasp strategies that exploit environmental constraints," in *IEEE International Conference on Robotics and Automation (ICRA)*. IEEE, 2015, pp. 4947–4952.
- [9] M. Mason, "The mechanics of manipulation," in *IEEE International Conference on Robotics and Automation (ICRA)*, vol. 2. IEEE, 1985, pp. 544–548.
- [10] M. R. Dogar and S. S. Srinivasa, "A framework for push-grasping in clutter," in *Robotics: Science and Systems*, vol. 2, 2011.
- [11] J. Lee, Y. Cho, C. Nam, J. Park, and C. Kim, "Efficient obstacle rearrangement for object manipulation tasks in cluttered environments," in *IEEE International Conference on Robotics and Automation (ICRA)*. IEEE, 2019, pp. 183–189.
- [12] J. E. King, M. Klingensmith, C. M. Dellin, M. R. Dogar, P. Velagapudi, N. S. Pollard, and S. S. Srinivasa, "Pregrasp manipulation as trajectory optimization," in *Robotics: Science and Systems*. Berlin, 2013.
- [13] K. Hang, A. S. Morgan, and A. M. Dollar, "Pre-grasp sliding manipulation of thin objects using soft, compliant, or underactuated hands," *IEEE Robotics and Automation Letters*, vol. 4, no. 2, pp. 662–669, 2019.
- [14] H. Liang, X. Lou, Y. Yang, and C. Choi, "Learning visual affordances with target-orientated deep q-network to grasp objects by harnessing environmental fixtures," in *IEEE International Conference on Robotics and Automation (ICRA)*. IEEE, 2021, pp. 2562–2568.
- [15] Z. Sun, K. Yuan, W. Hu, C. Yang, and Z. Li, "Learning pregrasp manipulation of objects from ungraspable poses," in *IEEE International Conference on Robotics and Automation (ICRA)*. IEEE, 2020, pp. 9917–9923.
- [16] W. Zhou and D. Held, "Learning to grasp the ungraspable with emergent extrinsic dexterity," in *Conference on Robot Learning*. PMLR, 2023, pp. 150–160.
- [17] S.-M. Yang, M. Magnusson, J. A. Stork, and T. Stoyanov, "Learning extrinsic dexterity with parameterized manipulation primitives," in *IEEE International Conference on Robotics and Automation (ICRA)*. IEEE, 2024, pp. 5404–5410.
- [18] A. D. Christiansen, "Manipulation planning for empirical backprojections," in *IEEE International Conference on Robotics and Automation (ICRA)*. IEEE Computer Society, 1991, pp. 762–763.
- [19] J. Ish-Shalom, "The funnel algorithm and task level robot control," in *IEEE International Conference on Robotics and Automation (ICRA)*, vol. 4. IEEE, 1987, pp. 25–32.
- [20] S. Akella, W. H. Huang, K. M. Lynch, and M. T. Mason, "Parts feeding on a conveyor with a one joint robot," *Algorithmica*, vol. 26, pp. 313–344, 2000.
- [21] A. S. Morgan, K. Hang, B. Wen, K. Bekris, and A. M. Dollar, "Complex in-hand manipulation via compliance-enabled finger gaiting and multi-modal planning," *IEEE Robotics and Automation Letters*, vol. 7, no. 2, pp. 4821–4828, 2022.
- [22] A. Bhatt, A. Sieler, S. Puhlmann, and O. Brock, "Surprisingly robust in-hand manipulation: An empirical study," in *Robotics: Science and Systems*, 2021.
- [23] N. C. Daffe, A. Rodriguez, R. Paolini, B. Tang, S. S. Srinivasa, M. Erdmann, M. T. Mason, I. Lundberg, H. Staab, and T. Fuhlbrigge, "Extrinsic dexterity: In-hand manipulation with external forces," in *IEEE International Conference on Robotics and Automation (ICRA)*. IEEE, 2014, pp. 1578–1585.
- [24] A. Sieverling, C. Eppner, F. Wolff, and O. Brock, "Interleaving motion in contact and in free space for planning under uncertainty," in *IEEE International Conference on Intelligent Robots and Systems (IROS)*. IEEE, 2017, pp. 4011–4073.
- [25] E. Páll and O. Brock, "Analysis of open-loop grasping from piles," in *IEEE International Conference on Robotics and Automation (ICRA)*. IEEE, 2021, pp. 2591–2597.
- [26] G. Subramani, M. Zinn, and M. Gleicher, "Inferring geometric constraints in human demonstrations," in *Conference on Robot Learning*. PMLR, 2018, pp. 223–236.
- [27] L. Shao, T. Migimatsu, and J. Bohg, "Learning to scaffold the development of robotic manipulation skills," in *IEEE International Conference on Robotics and Automation (ICRA)*. IEEE, 2020, pp. 5671–5677.
- [28] X. Li and O. Brock, "Learning from demonstration based on environmental constraints," *IEEE Robotics and Automation Letters*, vol. 7, no. 4, pp. 10 938–10 945, 2022.
- [29] N. Ratliff, M. Zucker, J. A. Bagnell, and S. Srinivasa, "Chomp: Gradient optimization techniques for efficient motion planning," in *IEEE International Conference on Robotics and Automation (ICRA)*. IEEE, 2009, pp. 489–494.
- [30] B. Wen, W. Yang, J. Kautz, and S. Birchfield, "Foundationpose: Unified 6d pose estimation and tracking of novel objects," in *Proceedings of the IEEE/CVF Conference on Computer Vision and Pattern Recognition*, 2024, pp. 17 868–17 879.
- [31] V. N. Nguyen, T. Groueix, G. Ponimatkin, V. Lepetit, and T. Hodan, "Cnos: A strong baseline for cad-based novel object segmentation," in *Proceedings of the IEEE/CVF International Conference on Computer Vision*, 2023, pp. 2134–2140.
- [32] J. A. Andersson, J. Gillis, G. Horn, J. B. Rawlings, and M. Diehl, "Casadi: a software framework for nonlinear optimization and optimal control," *Mathematical Programming Computation*, vol. 11, pp. 1–36, 2019.
- [33] K. Lynch, *Modern Robotics*. Cambridge University Press, 2017.
- [34] B. Calli, A. Singh, J. Bruce, A. Walsman, K. Konolige, S. Srinivasa, P. Abbeel, and A. M. Dollar, "Yale-cmu-berkeley dataset for robotic manipulation research," *The International Journal of Robotics Research*, vol. 36, no. 3, pp. 261–268, 2017.